AGU PUBLICATIONS

Geophysical Research Letters

RESEARCH LETTER
10.1002/2014GL061786

Key Points:
- Ship detection by altimeter waveform analysis used to create a 20 year database
- Analysis of the evolution of ship traffic from 1992 to 2012
- Traffic growth is fourfold with maximums in the Indian Ocean and China Seas

Correspondence to:
J. Tournadre,
jean.tournadre@ifremer.fr

Citation:
Tournadre, J. (2014), Anthropogenic pressure on the open ocean: The growth of ship traffic revealed by altimeter data analysis, *Geophys. Res. Lett.*, *41*, 7924–7932, doi:10.1002/2014GL061786.

Received 8 SEP 2014
Accepted 16 OCT 2014
Accepted article online 20 OCT 2014
Published online 17 NOV 2014

Anthropogenic pressure on the open ocean: The growth of ship traffic revealed by altimeter data analysis

J. Tournadre[1]

[1] Laboratoire d'Océanographie Spatiale, IFREMER, Plouzané, France

Abstract Marine ecosystems are under increasing anthropogenic pressures from marine and terrestrial activities. Ship traffic, the major cause of change in the open ocean, and its temporal evolution are still largely unknown because of lack of data. Altimeter data provide a new powerful tool to detect and monitor the ship traffic through a method of analysis of echo waveform. The archive of seven altimeter missions has been processed to create a two decade database of ship locations. The estimated annual density maps compare well with the ones obtained from Automatic Identification System. The ship traffic analysis shows a global fourfold growth between 1992 and 2012, the largest increase being observed in the Indian Ocean and the Chinese seas reflecting the world trade change. Although mainly concentrated along lanes, the traffic has a direct impact on the atmosphere, e.g., on the growth of tropospheric nitrogen dioxide in the Indian Ocean.

1. Introduction

Marine ecosystems are under increasing anthropogenic pressures from marine and terrestrial activities [*Halpern et al.*, 2007, 2008]. Thirty-eight categories of drivers of change have thus been developed ranging from river discharges to climate change. Assessing and prioritizing these different drivers is a difficult task due to the sparsity of data over vast regions of the ocean. This is particularly true in the open ocean where the main cause of change is the maritime traffic. Indeed, shipping can affect even very remote locations and be the major source of anthrogenic ecological pressure in these regions via fuel leaks, oil discharge, waste disposal, etc. [*Halpern et al.*, 2008]. Although the international maritime trade is well known through the general shipping lanes and economic statistics provided, for example, by the United Nations Conference on Trade and Development (UNCTAD, http://unctadstat.unctad.org/), there is a lack of knowledge in the actual global distribution of the ships, i.e., vessel density, and its evolution over time due to economics or other causes (including piracy).

Vessel density maps provide quantitative measure of global ship traffic allowing for improved understanding of economics trade trends as well as giving insight to the ecological pressures associated with shipping in the open ocean. Ships are powered by fossil fuel creating the main source of air pollution in the open ocean [*Richter et al.*, 2004; *de Ruyter de Wildt et al.*, 2012]. Precise vessel density maps could be used to improve the modeling of air pollutants over sea and their trends in atmospheric chemistry general circulation models [*Franke et al.*, 2009; *Vinken et al.*, 2014]. Ships are also one of the major sources of noise in the ocean [*Chapman and Price*, 2011; *McKenna et al.*, 2012] with potential threat to marine animals that depend on sound for myriad ecological functions or the possibility of sound detection of icebergs cracks [*Dziak et al.*, 2013] .

The main challenge in creating a global vessel density map is the capability of detecting ships in any region of the globe. Terrestrial Automatic Identification System (AIS) is really efficient to monitor the ship traffic in coastal regions but up to now the satellite-based AIS because the satellite coverage that was not dense enough did not provide a good coverage of the open ocean [*Luxspace*, 2008].

In a recent study, *Tournadre* [2007] demonstrated that any target emerging from the sea could have a detectable signature in the noise part (i.e., the portion of the echo waveform above the sea) of high-resolution satellite altimeter waveforms. This detection capability was also used to estimate the distribution of small icebergs in the Southern Ocean on a monthly basis [*Tournadre et al.*, 2012]. The detection algorithm can also be used to detect ships in the world ocean. The archive from seven past and present satellite altimeter missions has been processed to create a global database of ships covering two decades (1992–2012) and to estimate the annual vessel density over the global ocean.

The first section of the present paper presents the data used and describes the method of detection and the computation of the vessel density. The results are analyzed in the second section in terms of evolution of the ship traffic for the past two decades, and an example of the impact of traffic on the atmosphere is also presented.

2. Method of Detection and Data

2.1. Detection Method

The detection method, presented in detail by *Tournadre et al.* [2008] is here only summarized. An altimeter is a nadir-looking radar that emits short pulses that are backscattered by the sea surface. The altimeter measures the backscattered power as a function of time to construct the echo waveform from which the geophysical parameters are estimated. A detailed description of the principles of altimetry is given, for example, in *Chelton et al.* [2001].

A point target of height δ above sea level located at distance d from the satellite nadir will give an echo in an altimeter waveform at the time t_0 defined by *Powell et al.* [1993]

$$\frac{ct_0}{2} = -\delta + \frac{1}{2}\frac{a+H}{aH}d^2 = -\delta + \frac{d^2}{2H''} \tag{1}$$

where c is the speed of light, a the Earth's radius, H the satellite altitude, and $H'' = H/(1 + H/a)$ is the reduced satellite height. The echo waveform of a point target is thus purely deterministic, i.e., a parabola as a function of time when the satellite flies over the target.

A ship is detectable in echo waveforms when its echo time, t_0, lies within the time range during which the echo waveform is integrated and when its backscatter coefficient is significantly larger than the thermal noise of the sensor. For Jason-1 altimeter, this noise, estimated over more than 10 million waveforms has a mean value −8.5 dB with a standard deviation of 1.3 dB. The backscatter of a ship has to be larger than −4.6 dB to be detectable at a 3 standard deviation level [*Tournadre et al.*, 2008].

A signature of ship is always characterized by the parabolic shape defined by (1). The automated detection is based on the analysis of the convolution product C between a filter, F characteristic of a ship signature, and the thermal noise part of the waveforms.

$$C(k,l) = \sum_{n=1}^{30}\sum_{m=1}^{M_2} \sigma_0(k,l)F(k-n,l-m) \tag{2}$$

where k is the telemetry sample index, l the waveform index, and σ_0 the echo power. For each waveform of the detected parabola, the maximum of correlation $C(l)$ and its location $k^C_{\max}(l)$ (i.e., the range) and the maximum of backscatter, $\sigma_{\max}(l)$, and its location $k^\sigma_{\max}(l)$ are determined. A waveform is assumed to contain a ship signature if $C_{\max}(l)$ and $\sigma_{\max}(l)$ are larger than given thresholds C_1 and σ_1 determined empirically by analysis of hundreds of signatures.

2.2. Vessel Density Maps

The archives of past and present altimeter missions are analyzed to produce a vessel database containing the time, latitude, longitude, range, and backscatter of all the detected ships. As the number of altimeter data available on a regular grid increases poleward because of the inclination of satellite orbits, the number of detected ships is biased toward larger values at higher latitude. To get a homogeneous distribution, the probability of presence of ships is considered rather than the raw number of detections. This probability P of presence is simply the ratio of the number N of ships detected within a grid cell (i,j) by the number N_s of valid altimeter samples within the same grid cell during the same observation period, t,

$$P(i,j,t) = N(i,j,t)/N_s(i,j,t) \tag{3}$$

The probability in vessel/km^2 is the ratio of the probability P by the area A_{SW} of the altimeter footprint.

$$P_s(i,j,t) = \frac{P(i,j,t)}{A_{SW}} \tag{4}$$

The vessel density per grid cell is given by

$$D(i,j,t) = \alpha.P_s(i,j,t).S(i,j) \tag{5}$$

Table 1. Main Characteristics of the Radar Altimeters Used to Build the Ship Database

Mission	Time Period	Altitude (km)	Inclination	Beam Width	Frequency (GHz)	Numbers of Bins	Track Point	Bin Width (ns)	Waveform Frequency (Hz)	Repeat Period (Day)
ERS-1	1992–1996	784	98°	1.3°	13.8	64	32.5	3.03	20	35
ERS-2	1995–2003	784	98°	1.3°	13.8	64	32.5	3.03	20	35
Topex	1992–2005	1334	66°	1.1°	13.6	128	32.5	3.125	10	10
Jason-1	2002–2012	1334	66°	1.3°	13.6	104	32.5	3.125	20	10
Envisat	2002–2012	784	98°	1.3°	13.575	128	43	3.125	20	35
Jason-2	2008–	1334	66°	1.3°	13.5	104	32.5	3.125	20	10
Cryosat	2012–	717	90°	1.2°	13.575	128	34.5	3.125	20	30

where $S(i,j)$ is the area of grid cell (i,j). The α coefficient is a normalization coefficient set to obtain a global number of ships of 62,000 in 2009 [*Luxspace*, 2008].

The area of the altimeter footprint for the detection of vessel of 20 m mean deck height A_{SW} is the product of the altimeter along-track resolution and the range of distance from nadir over which a vessel can be detected. Using the relationship between the time of the echo, the distance from nadir, and the elevation of a target emerging from the sea given by *Tournadre et al.* [2008], the range of detection d of a ship is given by

$$\sqrt{(ct_0 + 2\delta)H''} \geq d \geq \sqrt{(ct_1 + 2\delta)H''} \tag{6}$$

where δ is the ship height and t_0 and t_1 are the time limits of the usable range of the noise part of the waveform. For Jason-1 and $\delta = 15$ m, $H = 1340$ km and $t_0 = -32 \times 3.125$ ns and $t_1 = -5 \times 3.125$ ns, then 6.3 km $> d >$ 3.3 km; thus, $A_{SW} \simeq 5.8 \times 3. \times 2$ km^2, where the factor 2 accounts for the left-right ambiguity of the detection.

2.3. Altimeter Data

The detection is based on the analysis of high-resolution waveforms from satellite-borne altimeters provided in the Sensor Geophysical Data Records of seven altimeters, i.e., ERS-1, Topex, ERS-2, Envisat, Jason-1, Jason-2, and Cryosat. For dual frequency altimeters such as Jason-1 or Envisat, the detection has been conducted on the Ku band waveforms only. Table 1 summarizes the main characteristics of the different altimeters: the lifetime of the satellite, the altitude and inclination of the orbit, the antenna beam width, the signal frequency, the number of telemetry bins of the waveform, the nominal track point, the bin width and the waveform frequency, and the repeat period of the orbit (i.e., the time interval after which the satellite repeats its path).

2.4. Merging the Different Altimeters

As seven altimeters with different characteristics, sensitivity and noise levels are used; it is necessary to intercalibrate the seven vessel densities to create a homogeneous time series. This is done by adjusting the global number of ships for the overlapping period between an altimeter and Jason-1 (chosen because it has the longest lifetime). For ERS-1 that ended before the Jason-1 launch, the intercalibration is conducted versus ERS-2 that has the same orbit and sensor characteristics. After intercalibration, the vessel densities are merged to produce a homogeneous time series. The merged product is obtained by a weighted sum of the individual products

$$D_m(i,j,t) = \sum_{k=1}^{n} D_k(i,j,t).C_k \tag{7}$$

where the weights C_k are given by

$$C_k = \frac{N_S^k(i,j,t)}{\sum_{k=1}^{n} N_S^k(i,j,t)} \tag{8}$$

where N_S^k is the number of valid data for the satellite k and n is the number of satellites available at time t.

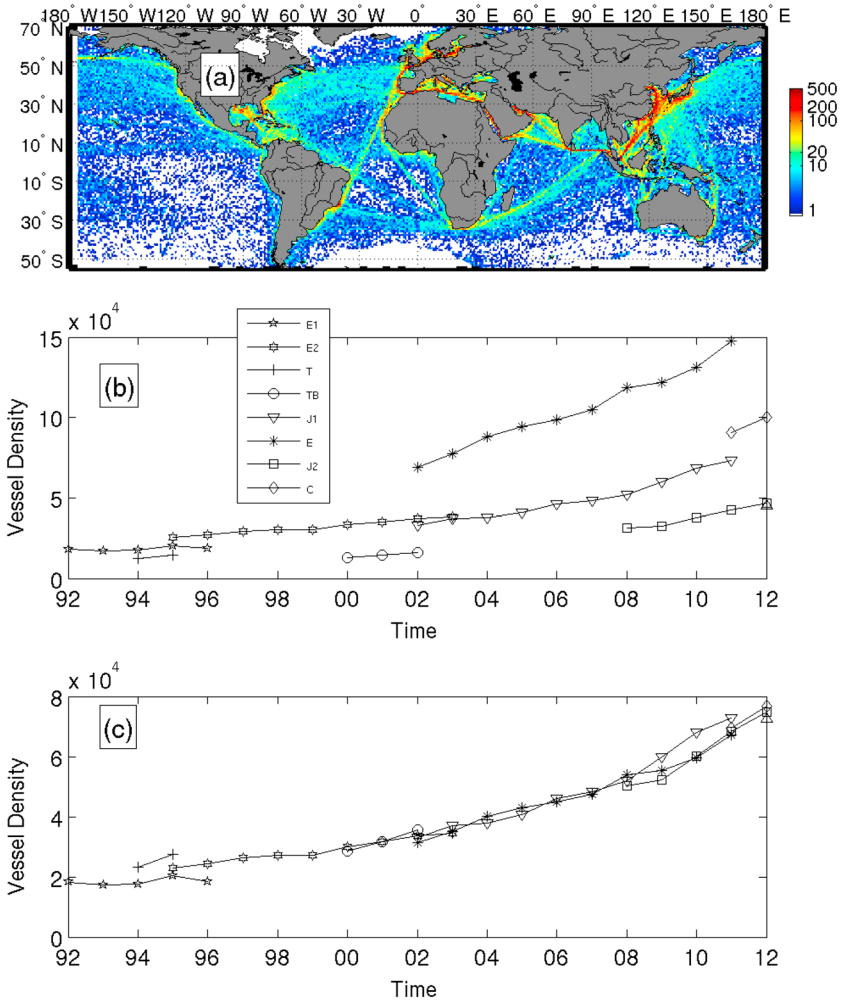

Figure 1. Number of ships detected during the 1992–2012 period (a) on a 1 × 1° grid (logarithmic scale). Global vessel density from the seven different altimeters between 1992 and 2012: (b) raw number and (c) calibrated numbers. E1: ERS-1, E2: ERS-2, T: Topex side A, TB: Topex side B, J1: Jason-1, E: Envisat, J2: Jason-2, C: Cryosat.

3. Ship Traffic From 1992 to 2012

More than 300,000 signatures were detected. Figure 1a that presents the number of detected ships, a 1 × 1° grid shows that the shipping lanes are well reproduced. Fixed targets corresponding to small islands, oil rigs, and lighthouses were detected in the data set and were screened using the database provided by National Center for the Ecological Analysis and Synthesis (available at http://www.nceas.ucsb.edu/globalmarine/impacts) [*Halpern et al.*, 2008]. Finally, icebergs were eliminated by using the extreme limit of icebergs [*Tournadre et al.*, 2012]. The number of ships detected by each altimeter is given in Table 2.

Table 2. Main Characteristics of the Radar Altimeters Used to Build the Ship Database

Mission	A_{SW} (km^2)	Calibration Coefficient/Jason-1	Detected Ships
ERS-1	27	1	6658
ERS-2	32	0.9	22513
Topex	31	1.9/2.2[a]	19775
Jason-1	35	1	67830
Envisat	38	0.45	102737
Jason-2	35	1.4	26793
Cryosat	19	0.77	13744

[a]Calibration of Topex sides A and B.

3.1. Ship Density

Altimeters are nadir-looking radar resulting in quite narrow swath (~30 km) (Table 2). This limited

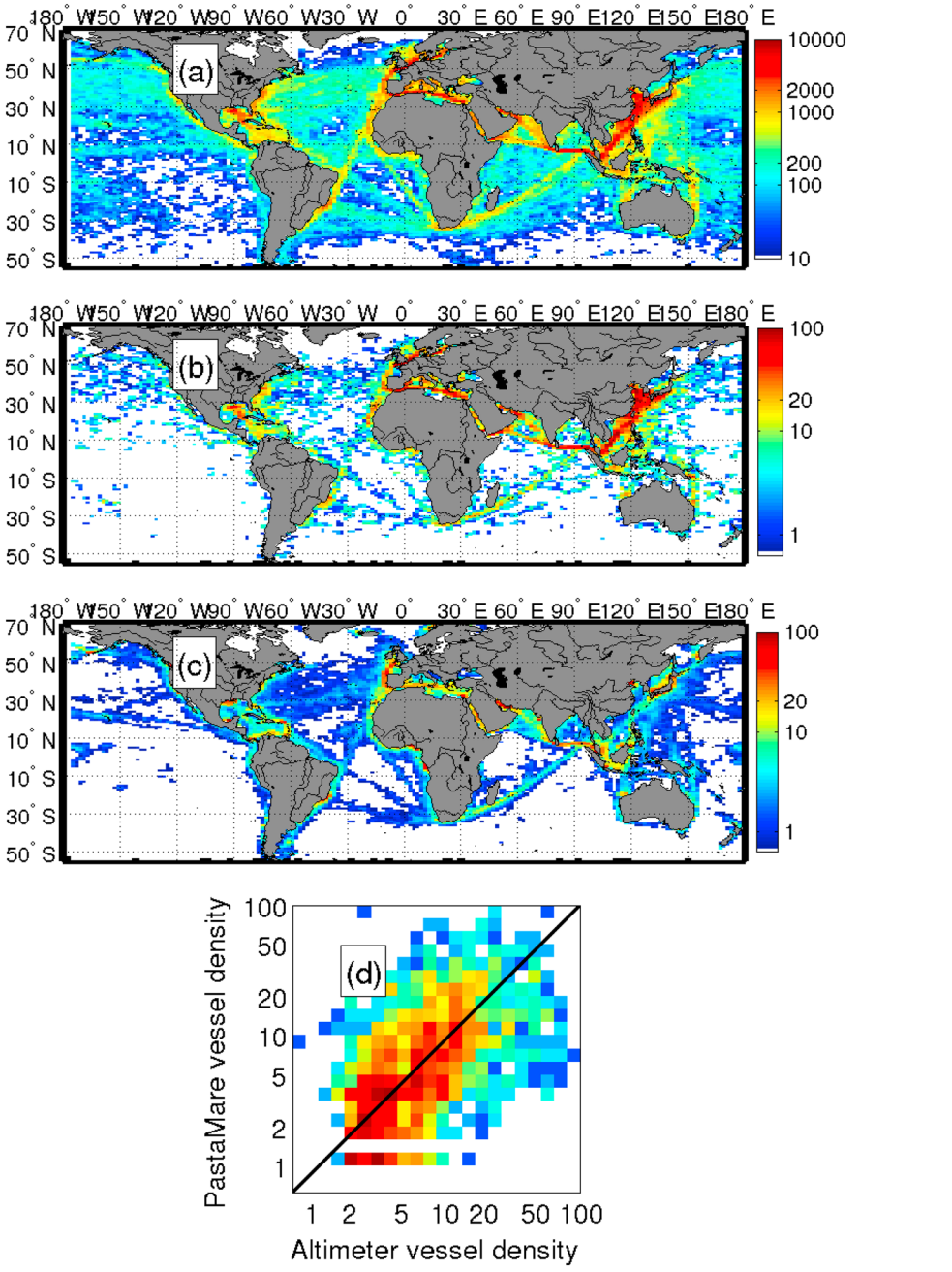

Figure 2. Mean merged vessel density during the 1992–2012 period (a) on a 1° × 2° grid. Vessel density (b) from altimeter and (c) from the PastaMare project for the November 2009 to February 2010 period. (d) Bidimensional histogram of PastaMare and altimeter vessel density from November 2009 to February 2010. The color scales are logarithmic.

coverage of the ocean does not allow to estimate the vessel density over short periods of time. This is particularly true for shipping lanes where traffic is low. To have enough ship detections, the vessel density is computed on an annual basis over a regular 1° × 2° latitude-longitude grid for each altimeter. Figure 1b presents the mean global ship density ($N(t) = \sum_i \sum_j N_V(i,j,t)$) estimated for each altimeter between 1992 and 2012.

The vessel densities are intercalibrated using the method of section 2.4. The coefficients of calibration are given in Table 2. Figure 1b and the calibration coefficients show that ERS-1, ERS-2, and Jason-1 have very similar detection capabilities. Envisat and Cryosat having a lower noise level and a better sensitivity detect significantly more ships than Jason-1 while Jason-2 has a lower detection capability.

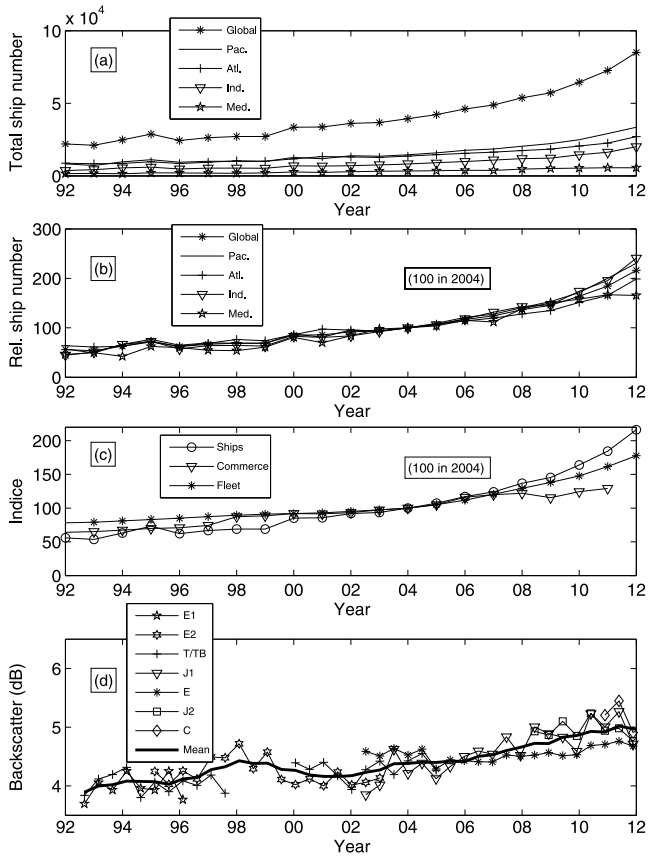

Figure 3. Annual ship number from 1992 to 2012 for the global ocean and the four ocean basins of Figure 4, (a) raw numbers, and (b) relative numbers with index 100 in 2004. (c) Comparison of the global ship number to the UNCTAD global trade and dead weight of the world fleet. (d) Evolution of the mean ship backscatter from the seven altimeters.

For Topex, starting in 1996, the aging of the instrument degraded the performance of the sensor and lead to an increase in the noise level of the waveforms that also slowly degraded the performances of the ship detection. In 1999, the switch to the backup TOPEX (side B) instrument was made. Because of the large noise level between 1996 and 1999, the Topex data cannot be used for ship detection and are eliminated from the database. As the Topex altimeter operated at a lower rate (10 Hz) than the other ones, it detects significantly fewer ships. The performances of the other sensors have been monitored, and the noise level did not significantly change during their lifetime.

The calibration ensures a good agreement between the seven estimates as it can be seen in Figure 1c, which presents the calibrated annual numbers of ships. These calibrated numbers are then used to compute the merged vessel density over the 20 year period using relation (7). The mean merged vessel density is presented in Figure 2a.

3.2. Validation

The vessel density is compared to the PastaMare project one (available at https://webgate.ec.europa.eu/maritimeforum/node/1603) for the October 2009 to February 2010 period. The PastaMare project uses AIS from both space-borne and terrestrial sensors to estimate the density in an approach similar to the altimeter ones. The Altimeter and PastaMare densities are presented in Figures 2b and 2c. Although the period considered is only 4 months long, the two densities are in good agreement. As expected, the lanes with little traffic are not very well represented in the altimeter density, but they contribute little to the global traffic. The PastaMare density appears to underestimate the traffic in the South China and Chinese seas maybe for technical reasons related to the AIS system. The bidimensional histogram of the two vessel densities shown in Figure 2d confirms the good overall agreement and shows that the altimeter data give comparable results to the AIS systems.

3.3. Evolution of the Ship Traffic

Figures 3a and 3b present the evolution of the ship density between 1992 and 2012 for the global ocean and the four ocean basins defined in Figure 4a. Between 1992 and 2002, the maritime traffic grew by 60% at a rather constant rate of about 6% yr^{-1}. After 2002 the growth steadily accelerates from 6% yr^{-1} to more than 10% yr^{-1} in 2011 with the exception of 2008–2009 when the traffic remains almost constant due to the economic crisis. In two decades, the global growth is fourfold (Figure 3b) and is even larger in the Indian and Pacific Oceans where the growth accelerates since 2008. On the other hand, the growth is reduced after 2008 in the Atlantic Ocean and the Mediterranean Sea.

The comparison with the UNCTAD international World annual seaborne trade and the dead weight of the world merchant fleet (Figure 3c) shows that the evolution of the ship traffic reflects both the growth of the international sea trade and the increase of the merchant fleet. However, the traffic, i.e., the average number

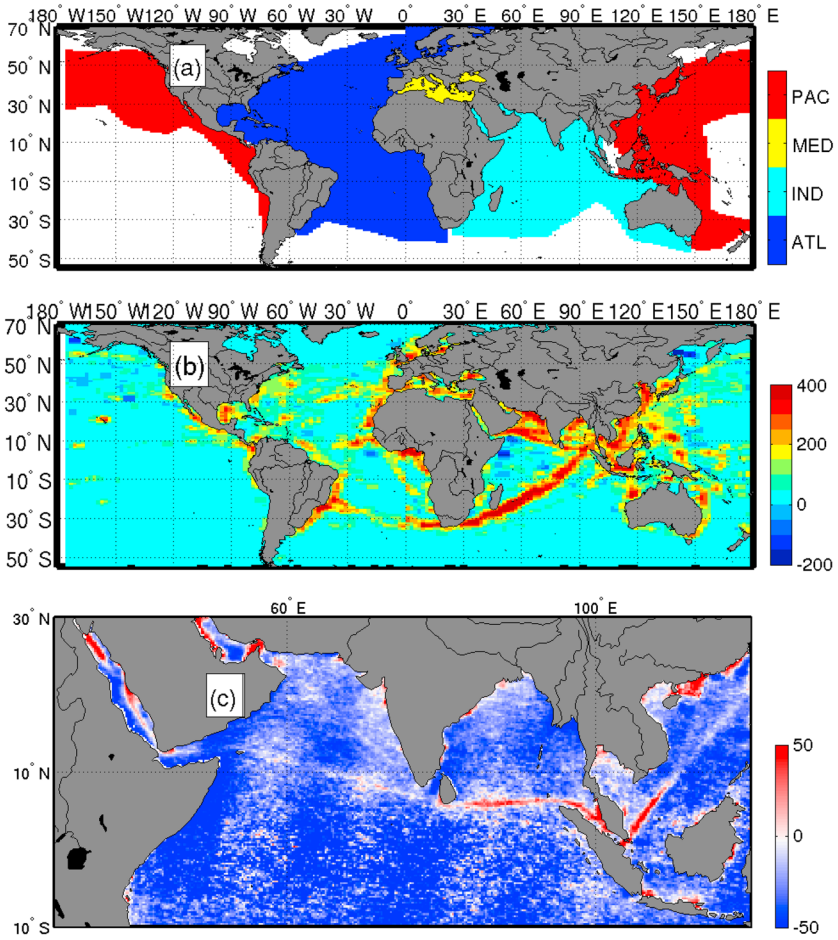

Figure 4. (a) Masks used for the Indian Ocean (light blue), the Pacific Ocean (red), the Atlantic Ocean (dark blue), and the Mediterranean Sea (yellow). (b) Evolution of ship traffic between 1992–2002 and 2003–2012 in percent. (c) Relative variation (in percent) of total columnar amount of tropospheric nitrogen dioxide between 1997–2003 and 2004–2010 from Global Ozone Monitoring Experiment (GOME) and Scanning Imaging Absorption Spectrometer for Atmospheric Chartography (SCIAMACHY).

of ship present at sea, appears to grow faster than the commerce and fleet since 2009. This can result for an increase of charters with less cargo and/or "slow steaming" and/or a higher ship detection probability resulting from the increase of the mean ship size [*Rodrigue et al.*, 2013]. Indeed, larger ships have a stronger radar backscatter and thus more easily detectable in the noise part of the altimeter waveforms. This can introduce a positive bias in the recent year. The mean annual backscatter of the detected ships remains quite stable for 1992–2005, and it steadily grows after 2005 reflecting an increase in the mean size of the detected ships that contributes to the increase of the ship traffic (Figure 3d). The observed growth might thus reflect both the growth of traffic and the better detection of vessels.

The difference (in percent) of vessel density between the 1993–2002 and 2003–2012 decades presented in Figure 4b shows that the traffic grows in all ocean basins except near the coast of Somalia where the development of piracy since 2006 almost completely halted commercial shipping. The growth is largest in the Indian Ocean especially in the Arabian Sea and the Bay of Bengal where the world's busiest lanes are concentrated. The pressure from ship traffic in these regions grows by more than 300% between the two decades. The growth is also important in the Chinese seas and in the west Pacific Seas reflecting the growing importance of the Asian trade while it is weaker, but still of the order of 100 to 200%, in the other basins with certainly larger impacts in closed seas, more sensitive to anthropogenic pressure such as the Mediterranean and Black Seas.

3.4. Impact on the Atmosphere

The vessel traffic is demonstrated to dramatically increase in the Indian Ocean especially on very well defined shipping lane like the Red Sea-Arabian Gulf-Asia one or the Asia-Cape Town route. Exhausts from ship engines are one of the main sources of air pollution in open ocean. The growth of traffic has a direct impact on the quantity of air pollutants that are easily detected in the variation of the mean total columnar amount of tropospheric nitrogen oxides (NO_x) between 1997–2003 and 2004–2010 from the GOME and SCIAMACHY monthly mean field [*Boersma et al.*, 2004] presented in Figure 4c. The increase of NO_2 associated with the ship traffic growth is especially strong along the Sri Lanka-Sumatra-China lane where the columnar amount grows by more than 50% . In the Arabian Sea the increase in pollution is more difficult to identify due to a general decreasing trend of NO_2, but the shipping lanes can still be identified as zone where the decrease is significantly lower.

4. Conclusion

In the open ocean, shipping is one of the major drivers (and in some regions the only one) of change with direct impact to the marine environment. Although the systems of ship identification and tracking have greatly improved in the recent years, it is still difficult to ascertain the distribution of traffic over the global ocean and its evolution. The development of new analysis techniques using high-resolution altimeter waveforms allows the detection of target (e.g., icebergs, lighthouses, and ships) emerging from the sea and the estimate of vessel density. Because of the limited swath of altimeter, the vessel density maps are estimated on an annual basis. The archive from seven past and present altimeter missions covers more than 20 years which allows a meaningful analysis in the growth and the pressure from the shipping industry to the ocean. Despite the complex altimeter sampling patterns and their small swaths, the altimeter vessel density compares very well with those obtained from AIS reports and compliments the other sources of data by its independent means of acquisition.

The analysis of the global ship density shows the dramatic fourfold increase of traffic between the early 1990s and present; even the 2008 economic crisis failed to slow down the trend. The only region that has a decline of traffic is located near Somalia and is related to piracy starting in 2006–2007. The distribution of the growth over the different ocean basins reflects the redistribution of the international trade with the largest growth in the Indian Ocean and the Western Pacific Seas. The traffic increase in the northern Atlantic and Pacific is somewhat more moderate but still between twofold and threefold. Enclosed seas such as the Mediterranean and the Black Seas that are certainly more sensitive to human factors are also under growing pressures.

Acknowledgments

The ERS-1, ERS-2, Envisat, and Cryosat altimeter data were provided by the European Space Agency. The Jason-1, Jason-2, data were made available by the AVISO center, while the Topex data were provided by NASA JPL. We acknowledge the free use of tropospheric NO_2 column data from the SCIAMACHY and GOME sensor from www.temis.nl. The study was partly funded by The French Centre National d'Etudes Spatiales. The author would like to thank the reviewers for their very constructive comments that greatly help to clarify and improve the text.

Peter Strutton thanks K. Boersma for assisting in evaluating this paper.

References

Boersma, K. F, H. J. Eskes, and E. J. Brinksma (2004), Error analysis for tropospheric NO_2 retrieval from space, *J. Geophys. Res.*, *109*, D04311, doi:10.1029/2003JD003962.

Chapman, N., and A. Price (2011), Low frequency deep ocean ambient noise trend in the Northeast Pacific Ocean, *J. Acoust. Soc. Am.*, *129*, EL161–EL165.

Chelton, D. E., J. C. Ries, B. J. Haines, L.-L. Fu, and P. S. c. Callahan (2001), Satellite altimetry, in *Satellite Altimetry and Earth Science: A Handbook of Techniques and Applications*, edited by L.-L. Fu and A. Cazenave, chap. 1, Academic Press, San Diego, Calif.

de Ruyter de Wildt, M., H. Eskes, and K. F. Boersma (2012), The global economic cycle and satellite-derived NO_2 trends over shipping lanes, *Geophys. Res. Lett.*, *39*, L01802, doi:10.1029/2011GL049541.

Dziak, R., M. Fowler, H. Matsumoto, D. Bohnenstiehl, M. Park, K. Warren, and W. Lee (2013), Life and death sounds of iceberg A53a, *Oceanography*, *26*(2), 10–12, doi:10.5670/oceanog.2013.20.

Franke, K., A. Richter, H. Bovensmann, V. Eyring, P. Jöckel, P. Hoor, and J. P. Burrows (2009), Ship emitted NO_2 in the Indian Ocean: Comparison of model results with satellite data, *Atmos. Chem. Phys.*, *9*, 7289–7301.

Halpern, B. S., K. A. Selkoe, F. Micheli, and C. V. Kappel (2007), Evaluating and ranking the vulnerability of global marine ecosystems to anthropogenic threats, *Conserv. Biol.*, *21*(5), 1301–1315, doi:10.1111/j.1523-1739.2007.00752.x.

Halpern, B. S., et al. (2008), A global map of human impact on marine ecosystems, *Science*, *319*, 948–952, doi:10.1126/science.1149345.

Luxspace (2008), Vessel density mapping, *Tech. Rep. Technical Note 4.1 Issue 4*, DG MARE Service Contract: No MARE/2008/06/ SI2.517298. [Available at https://webgate.ec.europa.eu/maritimeforum/content/1603.]

McKenna, M. F., S. L. Katz, S. M. Wiggins, D. Ross, and J. A. Hildebrand (2012), A quieting ocean: Unintended consequence of a fluctuating economy, *J. Acoust. Soc. Am.*, *132*, EL169–EL175, doi:10.1121/1.4740225.

Powell, R. J., A. R. Birks, W. J. Wrench, and C. L. Biddiscombe (1993), Using transponders with ERS-1 and Topex altimeters to measure orbit altitude to ± 3 cm, in *Proc. of the First ERS- Symposium (ESA SP-359)*, pp. 511–516, European Space Agency, Paris.

Richter, A., V. Eyring, J. P. Burrows, H. Bovensmann, A. Lauer, B. Sierk, and P. J. Crutzen (2004), Satellite measurements of NO_2 from international shipping emissions, *Geophys. Res. Lett.*, *31*, L23110, doi:10.1029/2004GL020822.

Rodrigue, J.-P., C. Comtois, and B. Slack (2013), *The Geography of Transport System,* 3rd ed., Routledge, New York.

Tournadre, J. (2007), Signature of lighthouses, ships, and small islands in altimeter waveforms, *J. Atmos. Oceanic Technol.*, *24*, 1143–1149.

Tournadre, J., K. Whitmer, and F. Girard-Ardhuin (2008), Iceberg detection in open water by altimeter waveform analysis, *J. Geophys. Res*, *113*, C08040, doi:10.1029/2007JC004587.

Tournadre, J., F. Girard-Ardhuin, and B. Legresy (2012), Antarctic icebergs distributions, 2002-2010, *J. Geophys. Res.*, *117*, C05004, doi:10.1029/2011JC007441.

Vinken, G. C. M., K. F. Boersma, A. van Donkelaar, and L. Zhang (2014), Constraints on ship NOx emissions in Europe using GEOS-Chem and OMI satellite NO2 observations, *Atmos. Chem. Phys.*, *14*, 1353–1369, doi:10.5194/acp-14-1353-2014.